A Trajectory-Driven SIMO mm-Wave Channel Model for a Moving Point Scatterer

Nurilla Avazov, Rym Hicheri, Matthias Pätzold,
Faculty of Engineering and Science, University of Agder, P.O.Box 509, 4898 Grimstad, Norway
E-mails: {nurilla.avazov, rym.hicheri, matthias.paetzold}@uia.no

Abstract—In this paper, we propose a trajectory-based three-dimensional (3D) non-stationary channel model for a millimeter wave (mm-Wave) single-input multiple-output (SIMO) system. The proposed channel model is designed to capture the mobility of a moving point scatterer in an indoor environment. We derive the expression of the time-variant (TV) channel transfer function (CTF). We study the TV Doppler characteristics of the channel, such as the TV Doppler power spectrum and the TV mean Doppler shift. To validate the proposed channel model, we performed a measurement campaign in an indoor environment using a software defined radar operating at 24 GHz. As a moving object, we consider a single swinging pendulum. The findings demonstrate an excellent agreement between the developed channel model and the real-world measured data. This can serve as a basis for developments of future non-stationary trajectory-driven channel models in the presence of moving objects modelled by multiple point scatterers.

Index Terms—Mean Doppler shift, mm-wave propagation, radar, spectrogram, time-variant channel models.

I. INTRODUCTION

Recently, human activity recognition (HAR) systems and services have received considerable attention of researchers around the world. HAR systems constantly emerge as the imaging and sensor technologies advances [1]. HAR systems can be classified into three groups, namely, computer vision-based [2], accelerometer-based [3], and radio-frequency-based systems [4]. Contrary to traditional wearable and context-aware HAR devices, radio-frequency-based systems, such as Wi-Fi and radar systems have several advantages. For example, radar-based systems are wearable-device free and human activities can be recognised based on the changes in the radio wave signal characteristics, such as range-Doppler profiles and micro-Doppler signatures [5]. Moreover, radar-based systems have better coverage compared to cameras, which have a limited viewing and require clear lighting conditions. Therefore, radar-based activity recognition methods have gained considerable attention from both academia and industry.

Recently, a new generation of radio-frequency-based activity recognition methods have been proposed [6], [7]. For instance, for detecting continuous human activity, Ding et al. [8] proposed a dynamic range-Doppler trajectory model based on a frequency-modulated continuous wave (FMCW) radar system. To locate and separate human activities, they applied a peak search method, and they analyzed the range-Doppler and radar cross-section characteristics. Kwon et al. [9] proposed a hands-free HAR framework based on millimeter wave (mm-Wave) sensors.

The proposed framework can remodel a human skeleton based on its motions.

Nevertheless, to characterize a wave propagation phenomenon in the presence of moving objects, there is a need for accurate channel models. The development of new channel models, which take into account the time-variant (TV) trajectories of moving objects as well as the positions of the transmit an receive antennas, allow us to emulate the non-stationary behaviour of indoor channels. Leveraging such channel models is the motivation of this paper. Channel models for HAR enable a paradigm shift from the experiment-based approach to the simulation-based approach for the design of HAR systems.

In this regard, a number of non-stationary channel models have been proposed in the literature to investigate the effect of TV Doppler characteristics caused by the mobility of scatterers [10], [11], [12]. For example, in [12] a three-dimensional (3D) non-stationary cluster-based channel model has been proposed for human activity recognition. Jost et al. [13] presented a geometry-based quasi-stationary channel model to describe the mobility of effective scatterers and a receiver. In [14], the effectiveness of the forward scattering radar (FSR) system for analysing the micro-Doppler signatures has been presented. Whereas, a wideband indoor channel model has been presented for the analysis of a micro-Doppler effect.

The aim of this paper is to model and investigate the impact of the motion of a point scatterer on the TV micro-Doppler power spectral characteristics of a 3D non-stationary indoor channel model. As a moving point scatterer, we consider a single pendulum swinging along a fixed direction. We derive the TV channel transfer function (CTF) for single-input multiple-output (SIMO) system and analyse its TV Doppler characteristics, such as TV micro-Doppler spectrogram and the TV mean Doppler shift. The proposed SIMO channel model is validated by real-world measurement data. The obtained results show that the proposed channel model has an excellent fit to the measured channel. The proposed channel model is a generic channel model in a way that by considering positions of different antenna elements and the presence of single moving object and multiple fixed objects it enables the characterization of the TV trajectory of the moving object. To the best of our knowledge, the impact of the distributed antenna configurations on the micro-Doppler spectrogram has not been studied.

In this regard, the key contributions of this paper are threefold. Firstly, we investigated the impact of the position of antenna

elements on the TV Doppler characteristics. Secondly, we presented a trajectory-based channel model for mm-Wave systems. Thirdly, we demonstrated the proof of concept by validating the proposed channel model with real-world measurement data.

The paper is structured as follows. Section II describes the geometrical channel model for an indoor scenario. The proposed TV stochastic channel model and the spectrogram analysis are presented in Section III and Section IV, respectively. The measurement and numerical results are provided in Section V. Finally, the conclusion is drawn in Section VI.

II. 3D INDOOR GEOMETRICAL MODEL

In the following, we consider the 3D propagation scenario depicted in Fig. 1, where the indoor environment is equipped with a $1 \times N_R$ SIMO system. The multipath propagation scenario in Fig. 1 consists of a single transmitter antenna A^T, multiple receiver antennas A_i^R ($i = 1, 2, \ldots, N_R$), K fixed objects S_k^F ($k = 1, 2, \ldots, K$), and a single moving object S^M. The transmitter antenna A^T is located at the fixed position (x^T, y^T, z^T), while the receiver antennas A_i^R have fixed positions (x_i^R, y_i^R, z_i^R) ($i = 1, 2, \ldots, N_R$). There is a single moving object modelled by a moving point scatterer S^M, which is represented by the red heptagon. Its position is described by the TV coordinates $x(t)$, $y(t)$, and $z(t)$. The trajectory $\mathcal{C}(t)$ of the moving object is defined by the TV coordinates $x(t)$, $y(t)$, and $z(t)$, i.e., $\mathcal{C}(t) = (x(t), y(t), z(t))$. As it is illustrated in Fig. 1, we denote by $d^T(t)$ ($d_i^R(t)$ $i = 1, 2, \ldots, N_R$) the TV Euclidean distance between the moving scatterer S^M and the transmitter (ith receiver) antenna A^T (A_i^R). The TV distance $d^T(t)$ can be expressed in terms of the TV coordinates $x(t)$, $y(t)$, and $z(t)$ of S^M as

$$d^T(t) = \sqrt{(x(t) - x^T)^2 + (y(t) - y^T)^2 + (z(t) - z^T)^2}. \quad (1)$$

Analogously, the TV Euclidean distance $d_i^R(t)$ is given by

$$d_i^R(t) = \sqrt{(x(t) - x_i^R)^2 + (y(t) - y_i^R)^2 + (z(t) - z_i^R)^2}. \quad (2)$$

The numerous fixed objects in the room (e.g., furniture, decoration items, walls) are modelled by K fixed scatterers S_k^F, which are at the fixed positions (x_k^F, y_k^F, z_k^F) ($k = 1, 2, \ldots, K$).
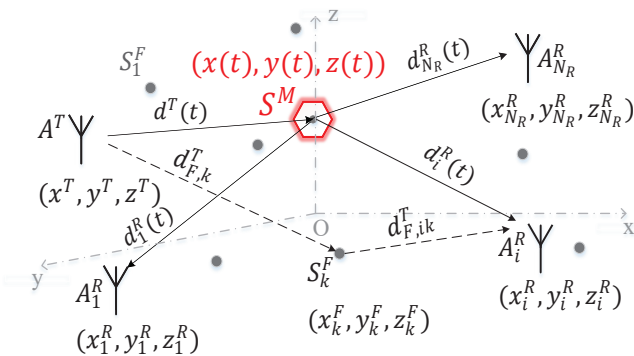

Fig. 1. 3D geometrical model for a $1 \times N_R$ SIMO system with a single moving scatterer S^M at position $(x(t), y(t), z(t))$ and K fixed scatterers S_k^F placed at (x_k^F, y_k^F, z_k^F) for $k = 1, 2, \ldots, K$.

The Euclidean distances between the fixed scatterer S_k^F and the transmitter and the receiver antennas are given by

$$d_k^T = \sqrt{(x_k^F - x^T)^2 + (y_k^F - y^T)^2 + (z_k^F - z^T)^2} \quad (3)$$

and

$$d_{i,k}^R = \sqrt{(x_k^F - x_i^R)^2 + (y_k^F - y_i^R)^2 + (z_k^F - z_i^R)^2}, \quad (4)$$

respectively.

III. CHANNEL MODEL

In this section, we derive the TV channel transfer function (TV-CTF) of a SIMO mm-Wave system. As illustrated in Fig. 1, the transmitted wave travels from the transmitter antenna A^T to the mobile (fixed) scatterer S^M (S_k^F) and impinges at the receiver antenna A_i^R. Hence, the TV-CTF of the link from A^T to A_i^R can be presented as follows:

$$H_i(t, f_q') = H_i^M(t, f_q') + \sum_{k=1}^{K} H_{i,k}^F(f_q') \quad (5)$$

where $H_i^M(t, f_q')$ and $H_{i,k}^F(f_q')$ denote the complex TV-CTF determined by the moving scatterer S^M and the fixed scatterer S_k^F, respectively. The symbol f_q', $q = 1, \ldots, Q$ stands for the qth subcarrier frequency, with Q being the total number of subcarriers. As we can see, the second term of (5) is time-invariant, which can be expressed as a superposition of K received multipath components caused by the K fixed scatterers. The two terms of the complex CTFs are given as follows:

$$H_i^M(t, f_q') = c_M e^{j[\theta_M - 2\pi(f_q' + f_c)\tau_i'^M(t)]} \quad (6)$$

$$H_{i,k}^F(f_q') = c_{F,k} e^{j[\theta_{F,k} - 2\pi(f_q' + f_c)\tau_{i,k}'^F]}. \quad (7)$$

In (6), the TV-CTF $H_i^M(t, f_q')$ is defined in terms of the fixed path gains c_M, phases θ_M, carrier frequency f_c, and the TV propagation delays $\tau_i'^M(t)$ of the moving scatterer, respectively. Similarly, the CTF $H_{i,k}^F(f_q')$ of the corresponding fixed scatterers is characterized by a fixed path gain $c_{F,k}$, the phase $\theta_{F,k}$ and the delays $\tau_{i,k}'^F$ associated with the fixed kth scatterer, respectively. It is noteworthy to mention that both phases θ_M and $\theta_{F,k}$ are independent and identically distributed (i.i.d.) random variables, each following the uniformly distribution over the range from $-\pi$ π. The TV propagation delay $\tau_i'^M(t)$ ($\tau_{i,k}'^F$) of the wave travelling from the transmitter antenna A^T to the receiver antenna A_i^R via the mobile (fixed) scatterer S^M (S_k^F) can be computed in terms of the Euclidean distances $d^T(t)$ (d_k^T) and $d_i^R(t)$ ($d_{i,k}^R$) as follows:

$$\tau_i'^M(t) = \frac{d^T(t) + d_i^R(t)}{c_0} \quad (8)$$

$$\tau_{i,k}'^F = \frac{d_k^T + d_{i,k}^R}{c_0} \quad (9)$$

where c_0 denotes the speed of light. The TV Doppler shift $f_i^M(t)$ of the moving object (scatterer) S^M can be computed by using the slope $\dot{\tau}_i'^M(t)$ of the TV delays $\tau_i'^M(t)$ such as $f_i^M(t) = -(f_q' + f_c)\dot{\tau}_i'^M(t)$ [15]. The TV delays $\tau_i'^M(t)$ are

determined by using the TV trajectory $\mathcal{C}(t) = (x(t), y(t), z(t))$ by means of the TV distances given in (1) and (2).

IV. SPECTROGRAM ANALYSIS

This section presents the Doppler characteristics of the proposed channel model, such as the TV Doppler spectrogram from which we can alternatively compute the TV mean Doppler shift.

The spectrogram analysis of the complex TV-CTF $H_i(t, f_q')$ is performed in the following four steps. First, we compute the complex channel gain $\mu_i(t)$ representing the ith channel link from A^T to A_i^R by computing the sample average of $H_i(t, f_q')$ w.r.t. f_q', i.e.,

$$\mu_i(t) = \frac{1}{Q} \sum_{q=1}^{Q} H_i(t, f_q') \tag{10}$$

where $i = 1, 2, \ldots, N_R$. Then, we multiply $\mu_i(t)$ by a sliding window function $w(t' - t)$ as follows:

$$x_i(t', t) = \mu_i(t) w(t' - t) \tag{11}$$

where $w(t)$ is a positive even function with normalized energy. Afterwards, we compute the short-time Fourier transform (STFT) of the complex channel gain $\mu_i(t)$ according to

$$X_i(f, t) = \int_{-\infty}^{\infty} x_i(t', t) e^{-i2\pi f t'} dt' . \tag{12}$$

Finally, we compute the squared magnitude of the STFT $X_H(f, t)$, which results in the spectrogram of the ith sub-channel

$$S_i(f, t) = |X_i(f, t)|^2 . \tag{13}$$

In this paper, we employ a Kaiser window function $w(t)$ given by

$$w(t) = \begin{cases} \dfrac{I_0\left\{ \beta \sqrt{1 - \left(\frac{2t}{T_0} - 1 \right)^2} \right\}}{I_0(\beta)}, & 0 \leq t \leq T_0 \\ 0, & \text{otherwise} \end{cases} \tag{14}$$

where T_0 stands for the window length and β determines the shape of window. The symbol $I_0(\cdot)$ denotes the modified Bessel function of the first kind of zero order.

By using the spectrogram $S_i(f, t)$ in (13), we can obtain the TV mean Doppler shift as follows

$$B_i^{(1)} = \frac{\int_{-\infty}^{\infty} f S_i(f, t) df}{\int_{-\infty}^{\infty} S_i(f, t) df} . \tag{15}$$

V. MEASUREMENT AND NUMERICAL RESULTS

In this section, we discuss the measurement campaign performed in a typical laboratory with a MIMO radar sensing system operating at 24 GHz. The radar system is an FMCW radar (Ancortek SDR-KIT 2400T2R4), which was attached to the white cabinet as shown in Fig. 2. The radar device is equipped with two transmitter and four receiver directional antennas. The radar transmits chirp signals with 250 MHz bandwidth and 1 ms chirp duration. The indoor environment

was a typical laboratory with a length of 11.5 m, width of 6 m, and height of 2.5 m as shown in Fig. 2. In the laboratory, we have fixed objects such as tables, chairs, and boards, and a single swinging pendulum as a mobile object. In our experiment, the pendulum was a medicine ball weighting 3 kg attached to the ceiling of a room by a rope with length L as illustrated in Fig. 2. Also, we employed SIMO configuration consisting of a single transmitter antenna and the three receiver antennas. The antennas are placed in the laboratory as depicted in Fig. 3. The first receiver antenna A_1^R and the transmitter antenna A^T are monostatically located at positions (x_1^R, y_1^R, z_1^R) and (x^T, y^T, z^T), respectively. The other two receiver antennas A_2^R and A_3^R are placed in a distributed manner as shown in Figs. 3 at positions (x_2^R, y_2^R, z_2^R) and (x_3^R, y_3^R, z_3^R), respectively. The list of geometrical model parameters, such as the maximum displacement $x_{\max}$, the length of the rope L, and the positions of the antennas, is presented in Table I.

Hence, by using the geometrical model parameters, we can compute the displacements $x(t)$, $y(t)$, and $z(t)$ of the pendulum as follows [16]:

$$x(t) = L \sin\left(\arcsin\left(\frac{x_{\max}}{L} \right) \cos\left(\sqrt{\frac{g}{L}} t \right) \right) \tag{16}$$

$$y(t) = 0 \tag{17}$$

$$z(t) = L\left\{ 1 - \cos\left[\arcsin\left(\frac{x(t)}{L} \right) \right] \right\} \tag{18}$$

where g and $x_{\max}$ denote the gravity acceleration and the maximum displacement, respectively. The displacements $x(t)$,

Fig. 2. Propagation environment in a laboratory.

TABLE I
MEASUREMENT SETTING PARAMETERS.

Model Parameters	Values and Units
(x^T, y^T, z^T)	(1, 0, 1.08) m
(x_1^R, y_1^R, z_1^R)	(1, 0, 1.08) m
(x_2^R, y_2^R, z_2^R)	(0.707, 0.707, 1.08) m
(x_3^R, y_3^R, z_3^R)	(0, -1, 1.08) m
L	1.52 m
$x_{\max}$	0.55 m

(a) $A^T - A_1^R$ link   (b) $A^T - A_2^R$ link   (c) $A^T - A_3^R$ link
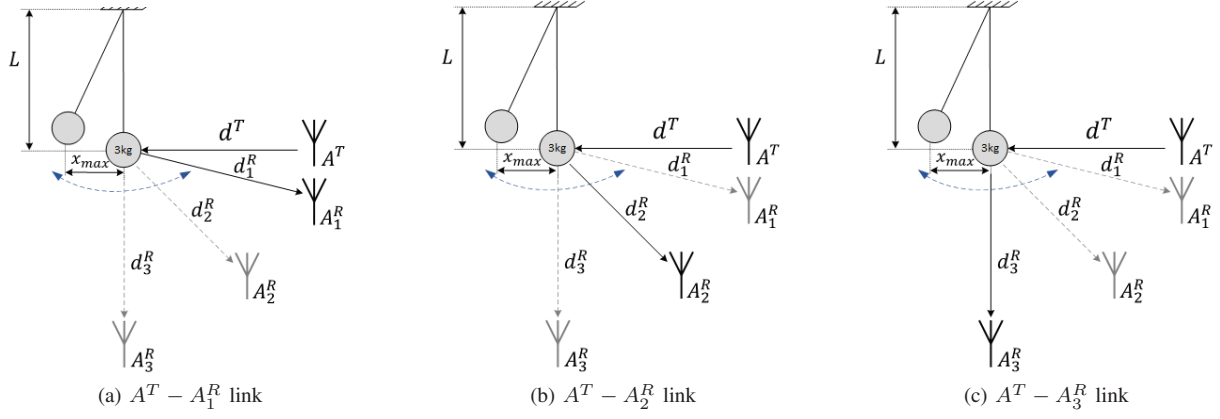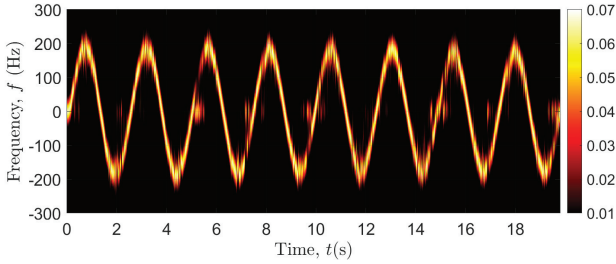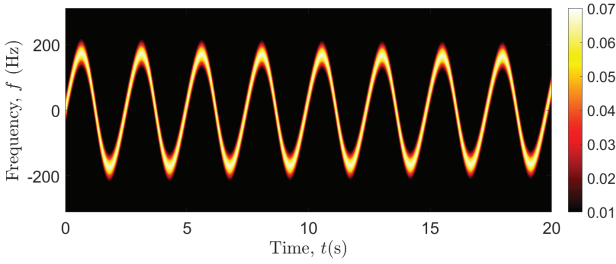
Fig. 3. Geometrical representations of the links: (a) $A^T - A_1^R$, (b) $A^T - A_2^R$, and (c) $A^T - A_3^R$, respectively.
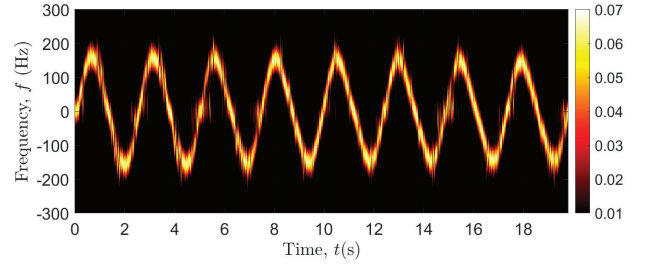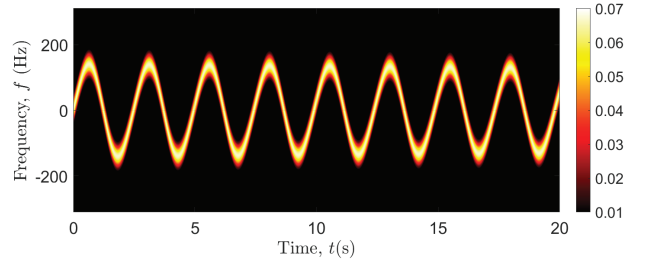

a)

b)

Fig. 4. (a) TV spectrogram $S_1^\star(f,t)$ of the measured received radar signal and (b) the spectrogram $S_1(f,t)$ of the mechanical-based channel model for the $A^T - A_1^R$ link.

a)

b)

Fig. 5. (a) TV spectrogram $S_2^\star(f,t)$ of the measured received radar signal and (b) the spectrogram $S_2(f,t)$ of the mechanical-based channel model for the $A^T - A_2^R$ link.

$y(t)$, and $z(t)$ form the trajectory of the swinging pendulum. In Fig. 3, we depict the geometrical representations of the three communication links.

Figures 4, 5, and 6 show the spectrograms of the measured $S_i^\star(f,t)$ and the simulated $S_i(f,t)$ channels for the links $A^T - A_1^R$, $A^T - A_2^R$, and $A^T - A_3^R$, respectively. The obtained results show that TV Doppler power characteristics of the measured channels and the proposed trajectory-driven channel models are almost identical. From Figs. 4–6, we can observe the impact of the different positions of A_i^R on the amplitudes of the Doppler frequencies. Due to the positions of the receiver antennas A_i^R w.r.t. the transmitter antenna A^T, we experience different TV distances, which in turns results in decreased amplitudes of the TV Doppler frequencies. Moreover, the excellent match in the spectrograms between the measured data and the analytical channel model illustrated in Figs. 4–6 confirms the validity

of the proposed model for different positions of the receiver antennas. For consistency purposes, we keep the same window function (14) which results in a "zig-zag" shaped spectrogram in Fig. 6. Furthermore, we studied the impact of the distributed antennas configuration on the TV mean Doppler shifts of the measured and simulated channels, which are presented in Fig. 7. As we discussed above, the position of A_i^R also influences the amplitude of the TV mean Doppler shift.

VI. CONCLUSION

In this paper, we proposed a trajectory-based 3D non-stationary channel model for distributed SIMO systems. We have derived the TV-CTF and studied the TV Doppler characteristics. To validate the proposed model, we performed a measurement campaign by using a SIMO radar in a laboratory, where a pendulum was acting as a point scatterer. The findings
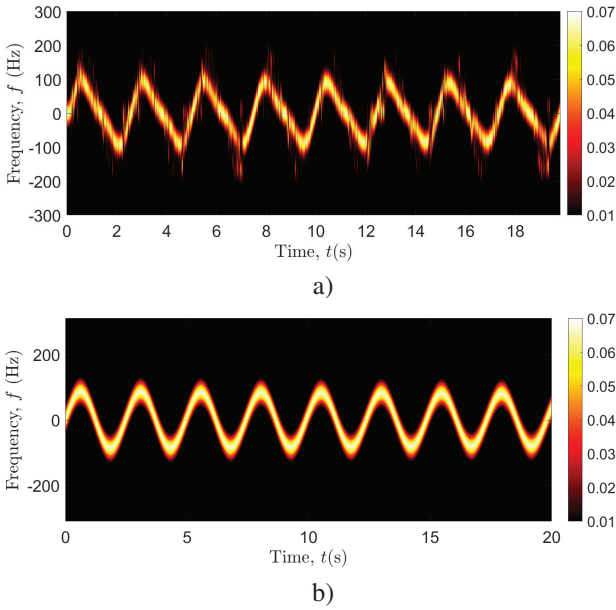
Fig. 6. (a) TV spectrogram $S_3^\star(f, t)$ of the measured received radar signal and (b) the spectrogram $S_3(f, t)$ of the mechanical-based channel model for the $A^T - A_3^R$ link.

demonstrate an excellent fit between the real-world measured data and the proposed channel model. Furthermore, we investigated the impact of the distributed antennas configurations on the micro-Doppler signatures of the received radar signal. The obtained results show that the position of the antenna elements are important for deeper understanding and analysis of the underlying activities. Thus, we believe that our proposed channel model can serve as a basis for analyzing the impact of moving objects within the indoor environments. In the future, the proposed model can be extended by considering moving objects modelled by multiple or a cluster of point scatterers, which can simulate human activities.

Fig. 7. The TV mean Doppler shift for the (a) $A^T - A_1^R$, (b) $A^T - A_2^R$, and (c) $A^T - A_3^R$ links, respectively.

REFERENCES

[1] J. Li, L. Tian, H. Wang, Y. An, K. Wang, and L. Yu, "Segmentation and recognition of basic and transitional activities for continuous physical human activity," *IEEE Access*, vol. 7, pp. 42 565–42 576, 2019.
[2] S. Zhang, Z. Wei, J. Nie, L. Huang, S. Wang, and Z. Li, "A review on human activity recognition using vision-based method," *Journal of healthcare engineering*, vol. 2017, 2017.
[3] D. Tao, L. Jin, Y. Yuan, and Y. Xue, "Ensemble manifold rank preserving for acceleration-based human activity recognition," *IEEE Trans. Neural Netw. Learn. Syst.*, vol. 27, no. 6, pp. 1392–1404, 2016.
[4] H. Fei, F. Xiao, J. Han, H. Huang, and L. Sun, "Multi-variations activity based gaits recognition using commodity WiFi," *IEEE Trans. on Veh. Tech.*, vol. 69, no. 2, pp. 2263–2273, 2020.
[5] V. C. Chen, F. Li, S. . Ho, and H. Wechsler, "Micro-Doppler effect in radar: phenomenon, model, and simulation study," *IEEE Transactions on Aerospace and Electronic Systems*, vol. 42, no. 1, pp. 2–21, 2006.
[6] W. Wang, A. X. Liu, M. Shahzad, K. Ling, and S. Lu, "Device-free human activity recognition using commercial WiFi devices," *IEEE J. Sel. Areas Commun.*, vol. 35, no. 5, pp. 1118–1131, May 2017.
[7] S. Wang and G. Zhou, "A review on radio based activity recognition," *Digital Communications and Networks*, vol. 1, no. 1, pp. 20–29, 2015.
[8] C. Ding, H. Hong, H. Zou, H. Chu, X. Zhu, F. Fioranelli, J. Le Kernec, and C. Li, "Continuous human motion recognition with a dynamic range-Doppler trajectory method based on FMCW radar," *IEEE Trans. on Geoscience and Remote Sensing*, vol. 57, no. 9, pp. 6821–6831, 2019.
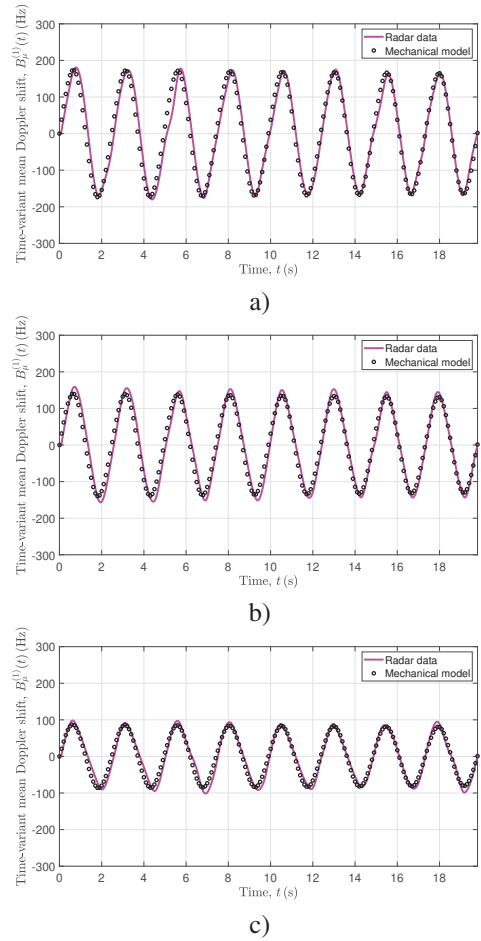[9] S. M. Kwon, S. Yang, J. Liu, X. Yang, W. Saleh, S. Patel, C. Mathews, and Y. Chen, "Demo: Hands-free human activity recognition using millimeter-wave sensors," in *2019 IEEE International Symposium on Dynamic Spectrum Access Networks (DySPAN)*, 2019, pp. 1–2.
[10] M. G. Amin, Y. D. Zhang, F. Ahmad, and K. C. D. Ho, "Radar signal processing for elderly fall detection: The future for in-home monitoring," *IEEE Signal Processing Magazine*, vol. 33, no. 2, pp. 71–80, 2016.
[11] J. Bian, C. Wang, M. Zhang, X. Ge, and X. Gao, "A 3-D non-stationary wideband MIMO channel model allowing for velocity variations of the mobile station," in *IEEE ICC*, May 2017, pp. 1–6.
[12] A. Abdelgawwad and M. Pätzold, "A 3D non-stationary cluster channel model for human activity recognition," in *2019 IEEE 89th Vehicular Technology Conference (VTC2019-Spring)*, April 2019, pp. 1–7.
[13] T. Jost, W. Wang, U. Fiebig, and F. Perez-Fontan, "Movement of equivalent scatterers in geometry-based stochastic channel models," *IEEE Ant. Wirel. Prop. Letters*, vol. 11, pp. 555–558, 2012.
[14] R. S. A. Raja Abdullah, A. Ali, S. A. Ahmad, R. N. Emileen, S. Aduwati, and P. Indin, "Micro-Doppler esimation and analysis of slow moving objects in forward scattering radar system," *MDPI, Remote Sensing*, vol. 9, no. 699, pp. 1–23, July 2017.
[15] M. Pätzold and C. A. Gutierrez, "Modelling of non-WSSUS channels with time-variant Doppler and delay characteristics," in *2018 IEEE Seventh International Conference on Communications and Electronics (ICCE)*. Hue, Vietnam, July 2018, pp. 1–6.
[16] A. Abdelgawwad, A. Borhani, and M. Pätzold, "Modelling, analysis, and simulation of the micro-Doppler effect in wideband indoor channels with confirmaiton throught pendulum experiments," *MDPI, Sensors*, vol. 20, no. 1049, pp. 1–18, Feb. 2020.